

Study of Charmed Baryons Decays and $D^0 \rightarrow K^0\pi^0$ Decay at Belle

Sergey Semenov (For the Belle Collaboration)*

ITEP, Moscow, Russia, B.Cheremushkinskaja 25, 117259

E-mail: ssemenov@iris1.itep.ru

ABSTRACT: We present measurements of $\Omega_c^0 \rightarrow \Omega^- \pi^+$ decay, the Cabibbo-suppressed decays $\Lambda_c^+ \rightarrow \Lambda^0 K^+$ and $\Lambda_c^+ \rightarrow \Sigma^0 K^+$ (both first observations), $\Lambda_c^+ \rightarrow \Sigma^+ K^+ \pi^-$ (seen with large statistics for the first time), $\Lambda_c^+ \rightarrow p K^+ K^-$ and $\Lambda_c^+ \rightarrow p \phi$ (measured with improved accuracy). Improved branching ratio measurements for the decays $\Lambda_c^+ \rightarrow \Sigma^+ K^+ K^-$ and $\Lambda_c^+ \rightarrow \Sigma^+ \phi$, which are attributed to the W-exchange diagrams, are shown. We report on the first evidence for $\Lambda_c^+ \rightarrow \Xi(1690)^0 K^+$ and set an upper limit on non-resonant decay $\Lambda_c^+ \rightarrow \Sigma^+ K^+ K^-$. A measurement of the ratio of D^0 decay rates into $K_L^0 \pi^0$ and $K_S^0 \pi^0$ final states is also presented. This ratio can be used to disentangle the Cabibbo favored $D^0 \rightarrow \bar{K}^0 \pi^0$ and doubly Cabibbo suppressed $D^0 \rightarrow K^0 \pi^0$ amplitudes, and contributes to constrain the strong phase $\delta_{K\pi}$ between $D^0 \rightarrow K^- \pi^+$ and $D^0 \rightarrow K^+ \pi^-$. The results reported here are based on a data sample of 23.6 fb^{-1} collected by Belle detector at the e^+e^- asymmetric collider KEKB.

hep2001

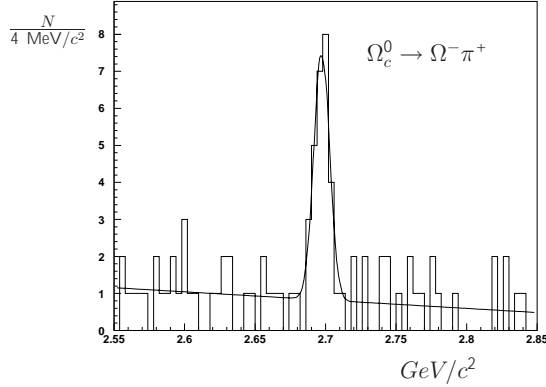
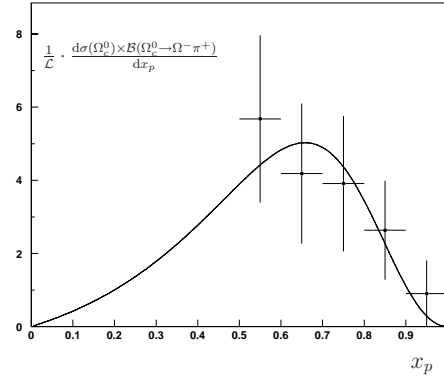
1. Measurement of the $\Omega_c^0 \rightarrow \Omega^- \pi^+$ decay

Fig. 1 shows the invariant mass distribution for the $\Omega^- \pi^+$ candidates¹. A clear peak is seen near $2700 \text{ MeV}/c^2$, while Ω^- sidebands show smooth behaviour in the mass region under consideration. A fit to the distribution with a gaussian for the signal (with width fixed to $5.7 \text{ MeV}/c^2$ from the MC) and a first order polynomial for the background yields 23.5 ± 5.4 events at a mass of $2697.3 \pm 1.5 \text{ MeV}/c^2$. The value of $\sigma(\Omega_c^0 | x_p > 0.5) \times \mathcal{B}(\Omega_c^0 \rightarrow \Omega^- \pi^+)$ is obtained to be $17.5 \pm 4.0 \text{ fb}$. The $\Omega_c^0 \rightarrow \Omega^- \pi^+$ decay was seen earlier by the E687[1] and CLEO[2] with 10.3 ± 3.9 and 13.3 ± 4.1 events correspondingly.

In order to extract the product of the production cross section and the branching ratio in the whole x_p interval, we fit the Ω_c^0 signal in five x_p bins. Peterson *et al.*[3] fragmentation function is used to fit the resulting spectrum for $x_p > 0.5$. The fit gives $\epsilon_p = 0.18_{-0.10}^{+0.27}$ from which we extrapolate $\sigma(\Omega_c) \times \mathcal{B}(\Omega_c \rightarrow \Omega^- \pi^+) = 24.2_{-13.8}^{+51.4} \text{ fb}$.

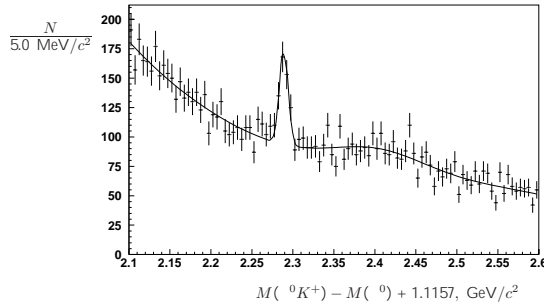
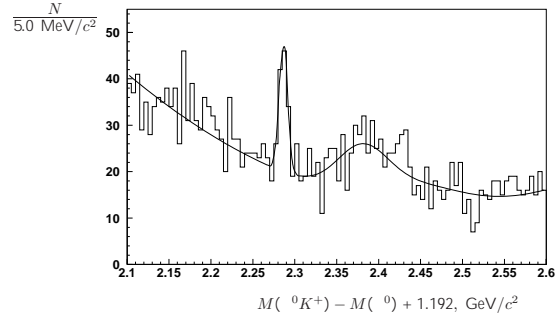
*Speaker.

¹Throughout the paper we implicitly include its charge conjugate when referring to a particular state

Figure 1: $\Omega^- \pi^+$ invariant mass distribution.Figure 2: x_p -distribution.

2. Observation of the $\Lambda_c^+ \rightarrow \Lambda^0 K^+$, $\Lambda_c^+ \rightarrow \Sigma^0 K^+$, $\Lambda_c^+ \rightarrow \Sigma^+ K^+ \pi^-$ decays

A clear peak in $\Lambda^0 K^+$ invariant mass distribution is shown in Fig. 3. The main background is associated with decays $\Lambda_c^+ \rightarrow \Sigma^0 \pi^+$ and $\Lambda_c^+ \rightarrow \Lambda^0 \pi^+$. Possible reflections from these

Figure 3: Invariant mass spectrum of the selected $\Lambda^0 K^+$ combinations.Figure 4: Invariant mass spectrum of the selected $\Sigma^0 K^+$ combinations.

channels and from Cabibbo-allowed Λ_c decays ($\Lambda_c^+ \rightarrow \Lambda^0 \pi^+ \pi^0$, $\Lambda_c^+ \rightarrow \Lambda^0 \pi^+ \pi^+ \pi^-$, $\Lambda_c^+ \rightarrow \Sigma^0 \pi^+ \pi^0$) are carefully studied using both by MC and data. The relative branching ratio is extracted to be $\mathcal{B}(\Lambda_c^+ \rightarrow \Lambda^0 K^+) / \mathcal{B}(\Lambda_c^+ \rightarrow \Lambda^0 \pi^+) = 0.085 \pm 0.012 \pm 0.015$.

Fig. 4 shows a clear peak in the invariant mass distribution for the selected $\Sigma^0 K^+$ candidates. Reflection due to misidentified two-body Cabibbo-allowed Λ_c^+ decays are seen at higher masses. The fit gives 70 ± 17 $\Lambda_c^+ \rightarrow \Sigma^0 K^+$ events. The ratio of branching ratios is found to be $\mathcal{B}(\Lambda_c^+ \rightarrow \Sigma^0 K^+) / \mathcal{B}(\Lambda_c^+ \rightarrow \Sigma^0 \pi^+) = 0.073 \pm 0.018 \pm 0.016$.

The invariant mass spectrum of $\Sigma^+ K^+ \pi^-$ combinations is shown in Fig. 5. The fit yields 72 ± 16 events. No enhancement is seen near the Λ_c^+ mass for Σ^+ sidebands (shaded histogram). The relative branching ratio calculated using the measured event yields is $\mathcal{B}(\Lambda_c^+ \rightarrow \Sigma^+ K^+ \pi^-) / \mathcal{B}(\Lambda_c^+ \rightarrow \Sigma^+ \pi^+ \pi^-) = 0.059 \pm 0.014$.

3. Measurement of the $\Lambda_c^+ \rightarrow \Sigma^+ K^+ K^-$ and $\Lambda_c^+ \rightarrow \Sigma^+ \phi$ decays

The decays $\Lambda_c^+ \rightarrow \Sigma^+ K^+ K^-$ and $\Lambda_c^+ \rightarrow \Sigma^+ \phi$ proceed dominantly via W-exchange diagrams, and were first observed by CLEO in 1993 [4]. The invariant mass spectrum of

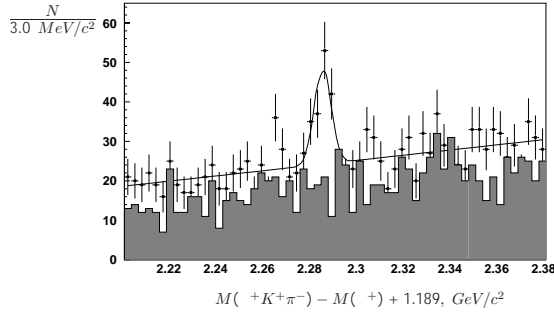


Figure 5: $\Sigma^+K^+\pi^-$ invariant mass spectrum; shaded histogram for the Σ^+ sidebands.

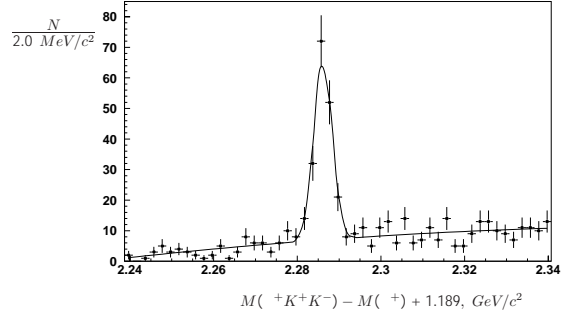


Figure 6: Invariant mass spectrum of the selected $\Sigma^+K^+K^-$ combinations.

$\Sigma^+K^+K^-$ combinations is shown in Fig. 6. The fit yields 161 ± 16 of $\Lambda_c^+ \rightarrow \Sigma^+K^+K^-$ decays. The relative branching ratio is $\mathcal{B}(\Lambda_c^+ \rightarrow \Sigma^+K^+K^-)/\mathcal{B}(\Lambda_c^+ \rightarrow \Sigma^+\pi^+\pi^-) = (7.5 \pm 0.8) \cdot 10^{-2}$.

In Fig. 7 we plot the K^+K^- invariant mass distribution for Λ_c candidates. The fit yields 106 ± 12 events for the ϕ signal in Λ_c^+ area and 15 ± 6 for the sidebands centered 10 MeV/ c^2 below and above the fitted Λ_c^+ mass (shaded histogram). After subtracting the sidebands we get $\mathcal{B}(\Lambda_c^+ \rightarrow \Sigma^+\phi)/\mathcal{B}(\Lambda_c^+ \rightarrow \Sigma^+\pi^+\pi^-) = (9.1 \pm 1.4) \cdot 10^{-2}$.

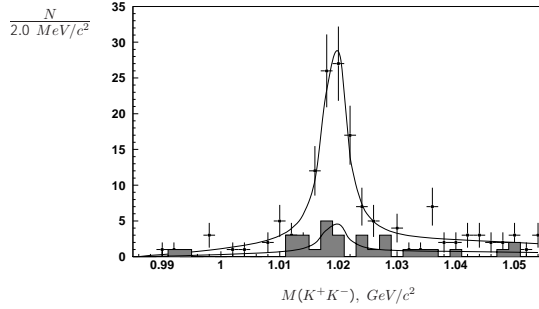


Figure 7: K^+K^- invariant mass spectra for events from the $\Lambda_c^+ \rightarrow \Sigma^+K^+K^-$ signal area (points with error bars) and sidebands (shaded histogram).

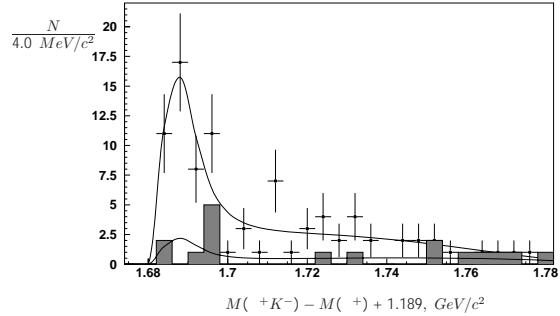


Figure 8: Σ^+K^- invariant mass spectra for events from the $\Lambda_c^+ \rightarrow \Sigma^+K^+K^-$ signal area (points with error bars) and sidebands (shaded histogram).

Fig. 8 shows the Σ^+K^- invariant mass spectra for $\Lambda_c \rightarrow \Sigma^+K^+K^-$ decays, where $|M(K^+K^-) - m_\phi| > 10$ MeV/ c^2 to suppress $\phi \rightarrow K^+K^-$. The shaded histogram represents Λ_c sidebands contribution. One can see an evidence of $\Xi(1690)^0$ resonant state. The histograms are fitted with a relativistic Breit-Wigner function (describing the $\Xi(1690)^0$ signal) plus the third order polynomial multiplied by the square root (to account for the mass threshold). The fit yields 52.5 ± 15.0 events for the $\Xi(1690)^0$ signal in Λ_c^+ area and 7.2 ± 2.8 for the sidebands contribution. This gives the relative branching ratio $\mathcal{B}(\Lambda_c^+ \rightarrow \Xi(1690)^0K^+) \times \mathcal{B}(\Xi(1690)^0 \rightarrow \Sigma^+K^-)/\mathcal{B}(\Lambda_c^+ \rightarrow \Sigma^+\pi^+\pi^-) = (2.1 \pm 0.7) \cdot 10^{-2}$, and the upper limit for non-resonant $\Lambda_c \rightarrow \Sigma^+K^+K^-$ decays $\mathcal{B}(\Lambda_c^+ \rightarrow \Sigma^+K^+K^-)_{non-res}/\mathcal{B}(\Lambda_c^+ \rightarrow \Sigma^+\pi^+\pi^-) < 0.014$ @ 90%CL.

4. Measurement of the $\Lambda_c^+ \rightarrow pK^+K^-$ and $\Lambda_c^+ \rightarrow p\phi$ decays

The invariant mass distribution of pK^+K^- combinations is shown in Fig. 9. The fit yields 446 ± 72 $\Lambda_c^+ \rightarrow pK^+K^-$ events and we obtain the branching ratio $\mathcal{B}(\Lambda_c^+ \rightarrow pK^+K^-)/\mathcal{B}(\Lambda_c^+ \rightarrow pK^-\pi^+) = (1.50 \pm 0.25) \cdot 10^{-2}$.

The invariant mass spectrum of K^+K^- combinations from $\Lambda_c^+ \rightarrow pK^+K^-$ is shown in Fig. 10; the equivalent distribution is also shown for Λ_c^+ sidebands (shaded histogram). The branching ratio is $\mathcal{B}(\Lambda_c^+ \rightarrow p\phi)/\mathcal{B}(\Lambda_c^+ \rightarrow pK^-\pi^+) = (1.50 \pm 0.23) \cdot 10^{-2}$.

Both measurements are more accurate than the most recent statistically significant resonant analysis published by CLEO [5].

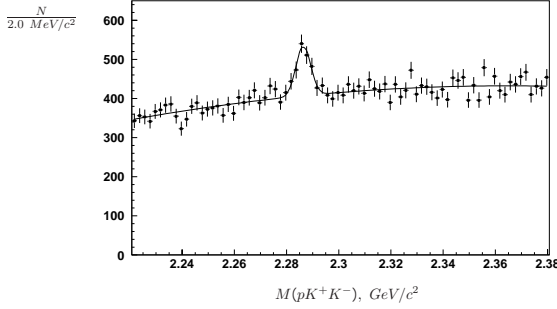


Figure 9: Invariant mass distribution of the pK^+K^- selected combinations.

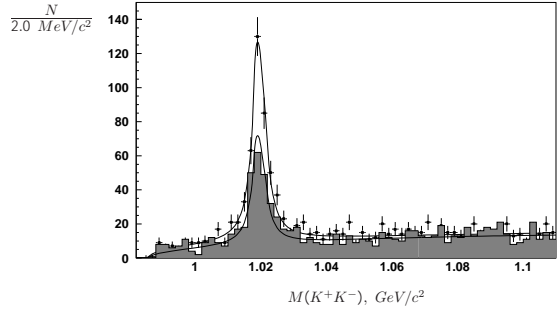


Figure 10: Invariant mass distributions of K^+K^- combinations from the $\Lambda_c^+ \rightarrow pK^+K^-$ signal area (points with error bars) and sidebands (shaded histogram).

5. Study of the $D^0 \rightarrow K^0\pi^0$ decay.

As has been shown in [6], new information on $\delta_{K\pi}$ may be obtained by measuring the asymmetry between the decay rates of D^0 into $K_S^0\pi^0$ and $K_L^0\pi^0$, where the effect may be as large as $\mathcal{O}(\tan^2 \theta_c)$. In order to cancel out most of the detector effects on the ratio of D^0 decay rates into $K_L^0\pi^0$ and $K_S^0\pi^0$ we extract the K_L^0/K_S^0 relative detection efficiency from the ratio of $K_L^0\pi^+\pi^-$ and $K_S^0\pi^+\pi^-$ modes via charged K^* . The presence of $K^* \rightarrow K^0\pi$ in the decay chain ensures equal rate of K_L^0 and K_S^0 in this mode.

The position of the shower in KLM or electromagnetic calorimeter gives information about the flight direction of the K_L^0 . To extract the *magnitude* of the K_L^0 momentum we apply a D^0 mass constraint and solve the resulting 4-momentum equation w.r.t. the magnitude of the K_L^0 momentum, and then exploit $D^* \rightarrow D^0\pi$ decay to tag the signal.

The resulting D^* mass plots for the four D^0 decay modes under study are shown in Fig.11. Our preliminary measurement of this ratio is

$$\frac{\mathcal{B}(D^0 \rightarrow K_L^0\pi^0)}{\mathcal{B}(D^0 \rightarrow K_S^0\pi^0)} = 0.88 \pm 0.09(\text{stat}) \pm 0.09(\text{syst}).$$

which is consistent with unity and at the current level of precision does not allow to uniquely determine the value of the phase difference between CF and DCS amplitudes. However

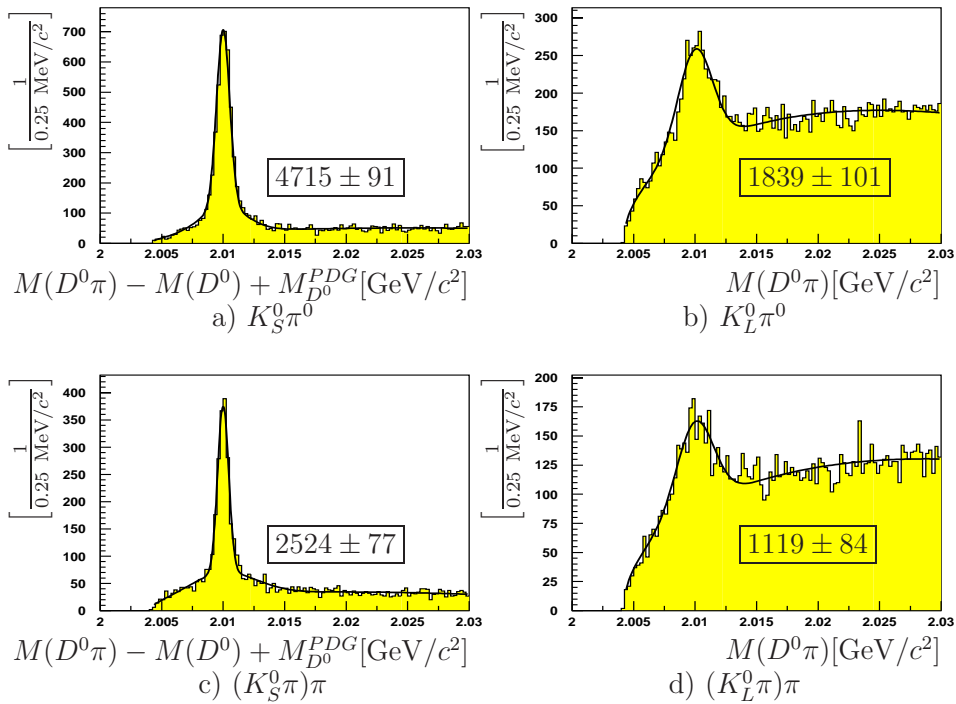


Figure 11: D^* mass plots for the specified D^0 decay modes

the statistical error will soon improve as more data is accumulated by the Belle detector. As for the systematic error, it is currently dominated by the inaccuracy in the background parametrization and could be diminished.

Acknowledgments

I would like to thank all members of the BELLE collaboration. I am grateful to R. Chistov, V. Eiges and R. Kagan for their assistance in preparing this talk.

References

- [1] P.L.Frabetti *et al.*, *Phys. Lett.* **B 300** (1993) 190.
- [2] D. Cronin-Hennessy *Phys. Rev. Lett.* **86** (2001) 3730.
- [3] C.Peterson *et al.*, *Phys. Rev.* **D 27** (1983) 105.
- [4] P. Avery *et al.*, *Phys. Rev. Lett.* **71** (1993) 2391.
- [5] J. Alexander *et al.*, *Phys. Rev.* **D 53** (1996) 1013.
- [6] E. Golowich and S. Pakvasa, *Phys. Lett.* **B 505** (2001) 94.